

Pruned Volterra-Based Distortion Mitigation of High-Speed GaN Micro-LEDs for Energy-Efficient Optical Communication

Enzo Barzan^{1,2}, Luc Maret¹, Nicolas Delaunay¹, Mahmoud Chakaroun^{2,3}, and Alexis P.A. Fischer^{2,3}

¹Université Grenoble Alpes, CEA-LETI, 17 Rue Des Martyrs, 38054 Grenoble, France

²Laboratoire de Physique des Lasers, UMR CNRS 7538, Université Sorbonne Paris Nord, 93430 Villetaneuse, France

³Centrale de Proximité en Nanotechnologies de Paris Nord, Université Sorbonne Paris Nord, 93430 Villetaneuse, France

Abstract—High-speed micro light-emitting diodes (LEDs) are attractive candidates for optical communications (OC) due to their wide bandwidth and energy efficiency. However, their strong nonlinear distortion severely degrades system performance. In this work, we present the first adaptation of the generalized memory polynomial model to micro-LED-based OC and propose a second approach based on a novel pruned Volterra model. Training and validation of the models are performed using digital postdistortion. Experimental validation on gallium nitride micro-LEDs driven by direct current-biased optical orthogonal frequency division multiplexing shows significant improvements, including a 71% throughput increase, from 4.32 Gb/s to 7.38 Gb/s. These results demonstrate the strong potential of these compensation schemes to unlock energy-efficient, high-speed micro-LED optical links.

Index Terms—digital predistortion, digital postdistortion, optical communication, micro-LED, memory effects, OFDM, Volterra model, Volterra pruning, generalized memory polynomial

I. INTRODUCTION

Optical communication (OC) has a lot of benefits over traditional radio frequency (RF) communication, including enhanced security, license-free spectrum, reduced size, weight and power consumption of transmission devices. Furthermore, OC has received renewed interest with the development of high-speed micro light-emitting diodes (LEDs), which allow transmissions over much wider bandwidths than macro-LEDs. While throughput has often been the driving factor in system design, at the cost of considerable energy consumption, current studies are shifting toward sustainability and improved energy efficiency. A comparison of recent advancements in micro-LED based visible light communication systems is summarized in Table I. However, many challenges come with this transmission source, one of them being nonlinear distortion, impacting throughput and energy efficiency. More specifically, micro-LED distortion can be divided into two main contributions: static nonlinear behavior and memory effects, with the latter growing stronger as the devices' bandwidths get larger [1]. The problem becomes more challenging when dealing with orthogonal frequency division multiplexing (OFDM) since the resulting time signal often has a high peak-to-average

power ratio (PAPR), which increases the signal excursion and the amount of distortion. Plenty of studies have been conducted on power amplifiers (PAs) in order to reduce the impact of the distortion in RF systems. However, few papers have been published on OC and fewer on micro-LED-based optical communication. Famous distortion compensation schemes for PAs include digital predistortion (DPD) and digital postdistortion (DPoD), which consists in applying an “inverse” distortion function just before the digital-to-analog converter (or just after the analog-to-digital converter, respectively) in order to obtain a linear response from the whole system. This linearization improves the signal to noise ratio (SNR), which in turn improves throughput, energy efficiency and transmission range. Linearization also allows for a wider range of the direct current (DC) bias voltage, which is beneficial to the joint optimization of throughput and energy efficiency. Many linear DPD models have been developed for RF communication, including the memory polynomial (MP) model [2], [3], the generalized memory polynomial (GMP) model [4], [5], and other Volterra-based models [6], [7]. The MP model was applied to compensate micro-LED distortion in [8], while the GMP model has only been applied to laser diodes (LDs)-based OC [9], [10]. Finally, a Volterra-based model has been applied to micro-LED distortion mitigation by Sun et al. in [11], resulting in a throughput and energy efficiency gain of 25%.

The current work presents additional gains in throughput and energy efficiency through two novelties: firstly, the GMP model is applied to micro-LED-based OC for the first time resulting in greater gains compared to [11], and secondly the introduction of a novel Volterra-based model leading to even more throughput gain and more robustness than the GMP model.

II. DISTORTION MITIGATION SCHEMES

To linearize the system and properly compensate micro-LED distortion, we must first select a model able to learn the distortion pattern and train it to behave as the inverse

TABLE I
COMPARISON OF PERFORMANCES OF RECENT VISIBLE LIGHT COMMUNICATION SYSTEMS.

| Year | LED type | Size | Throughput | Signal bandwidth | Energy efficiency | DPD/DPOd gain | Modulation | Ref |
|-------------|-----------------|------------------------------------|------------------|------------------|-------------------|---------------|-------------|------------------|
| 2017 | Violet GaN | 40 μm | 7.91 Gb/s | 1.81 GHz | 19 pJ/bit | - | OFDM | [12] |
| 2021 | Blue GaN | 75 μm | 8.75 Gb/s | 1.025 GHz | 19 pJ/bit | - | OFDM | [13] |
| 2022 | UVC AlGaIn | 40 μm | 6.94 Gb/s | 1.45 GHz | 61 pJ/bit | - | OFDM | [14] |
| 2023 | Green GaN | 80 μm | 6.04 Gb/s | 1 GHz | 106 pJ/bit | 25% | OFDM | [11] |
| 2023 | Blue GaN | 60 μm | 10.55 Gb/s | 2.3 GHz | 188 pJ/bit | - | OFDM | [15] |
| 2025 | Blue GaN | 40 μm | 7.38 Gb/s | 1.875 GHz | 40 pJ/bit | 71% | OFDM | This Work |

distortion function. In this section, we present three DPD models with different memory structures before comparing their performances in Section IV. While the MP and GMP models have been widely presented in the literature, this work introduces a version of these models adapted to micro-LED distortion mitigation.

A. Adapted memory polynomial model

The MP model is a behavioral model widely used in PA distortion mitigation:

$$\hat{y}(n) = \sum_{p=1}^P \sum_{m=0}^M w_{p,m} x(n-m)^p \quad (1)$$

with:

- x the input,
- \hat{y} the estimated output,
- $w_{p,m}$ the model coefficients,
- P the model order,
- M the model memory depth.

This version of the MP model differs from those in the literature, as in [2], [3], in that the absolute value has been removed. Indeed, since the original model is designed for modeling and distortion mitigation of PAs, which exhibit odd-symmetric behavior regardless of signal polarity, the use of symmetrical envelopes provides a more accurate fit. However, micro-LEDs do not behave similarly and usually do not show any exploitable symmetry in their distortion.

This model is one way to combine memory and polynomial expansion which can only model distortion in-phase with the signal, making it only suitable for systems with limited distortion.

B. Adapted generalized memory polynomial model

The GMP model has been applied to PA distortion mitigation for decades. Although micro-LEDs exhibit some similar nonlinearities, it has only been applied to LD-based OC for few years [9]. This paper presents the first adaptation of the GMP model to the distortion mitigation of micro-LED-based OC.

The enhanced GMP model is an extension of the MP model with added cross-terms:

$$\hat{y}(n) = \sum_{p=1}^{P_a} \sum_{m=0}^{M_a} a_{p,m} x(n-m)^p + \quad (2)$$

$$\sum_{p=1}^{P_b} \sum_{m=0}^{M_b} \sum_{l=1}^{L_b} b_{p,m,l} x(n-m)x(n-m-l)^p + \quad (3)$$

$$\sum_{p=1}^{P_c} \sum_{m=0}^{M_c} \sum_{l=1}^{L_c} b_{p,m,l} x(n-m)x(n-m+l)^p \quad (4)$$

with:

- $a_{p,m}$, $b_{p,m,l}$, $c_{p,m,l}$ the model coefficients,
- P_a , P_b , P_c the model orders,
- M_a , M_b , M_c the model memory depths,
- L_b , L_c the shift values of the envelopes.

Similar to the MP model presented in Section II-A, this version of the GMP model differs from those in the literature, as in [4], [5], in that the absolute value functions have been removed. This proposed GMP model is an adapted version of the regular GMP model applied to micro-LED distortion mitigation.

The model can be divided into three terms: the MP term (2), modeling distortion in-phase with the original signal (aligned envelope), the lagging envelope terms (3) and the leading envelope terms (4), modeling modulations typically caused by memory effects with different time scales.

C. Novel pruned Volterra model

The Volterra models derive from the Volterra series, which can be seen as a generalization of the convolution for higher orders or as an equivalent of the Taylor expansion for systems with memory:

$$\hat{y}(n) = \sum_{p=1}^P \sum_{m_1=a_1}^{b_1} \dots \sum_{m_p=a_P}^{b_P} h_p(m_1, \dots, m_p) \prod_{j=1}^p x(n-m_j) \quad (5)$$

with:

- $h_p(m_1, \dots, m_p)$ the Volterra kernels (model coefficients), representing higher-order impulse responses of the system,
- P the model nonlinearity order,
- a_1, \dots, a_P and b_1, \dots, b_P the domain bounds.

If $a_1, \dots, a_P > 0$, the output only depends on the current and previous samples, and the Volterra model is said to be causal.

While this model is very powerful in representing nonlinear systems with memory, its complexity scales exponentially, leaving only low-order Volterra models accessible for practical implementation.

Another way of reducing computational cost is pruning, which consists in discarding specific terms according to a set of specified rules. Several pruning methods have been developed for PAs [16], [17]. A second-order Volterra model for micro-LED distortion mitigation has been studied in [11].

This current work presents a novel Volterra pruning method based on the GMP model, which already achieved a close fit to the micro-LED distortion pattern. This pruning method allows the new model to inherit the GMP structure while allowing other related basis functions in the model to reach a more precise fit. All the redundant terms are also removed from the model to reduce multicollinearity and enhance conditioning of the model design matrix, making model training easier and more robust. Since the kernels of the Volterra series are symmetrical due to the commutativity of the multiplication, we can remove redundant terms by writing the series in a triangular form.

To build the model presented in this work, we start from a non-causal Volterra model with varying memory depths and a triangular form for each order:

$$\hat{y}(n) = \sum_{m_1=-A_1}^{M_1} h_1(m_1)x(n-m_1) + \sum_{m_1=-A_2}^{M_2} \sum_{m_2=m_1}^{M_2} h_2(m_1, m_2)x(n-m_1)x(n-m_2) + \dots + \sum_{m_1=-A_P}^{M_P} \dots \sum_{m_P=m_{P-1}}^{M_P} h_P(m_1, \dots, m_P) \prod_{j=1}^P x(n-m_j) \quad (6)$$

with:

- $A_1, \dots, A_P > 0$ and $M_1, \dots, M_P > 0$ the domain bounds.
- We then apply two pruning rules:
- No more than two distinct factors for each term.
 - One of the factors is of order 1.

Every component of this model can then be written in the form:

$$\prod_{j=1}^p x(n-m_j) = x(n-m_a)x(n-m_b)^k$$

with $(m_a, m_b) \in \mathbb{Z}^2, k \in \mathbb{N}$.

These rules are inspired by the GMP model structure presented in Section II-B, but they lead to a broader model than the GMP for the same nonlinear order and memory depth.

The GMP model is designed to represent static nonlinearities (memoryless terms) as well as fast and slow dynamical nonlinearities (in-phase envelope terms and shifted-envelope terms, respectively). This allows behavioral models such as the GMP model to efficiently mitigate these distortions regardless of their physical origin.

By design, the novel proposed Volterra model includes all the terms of the GMP model and therefore inherits the

corresponding modeling capabilities, while its construction allows for finer control and a broader exploration of the functional space within each nonlinear order. In particular, since second-order Volterra kernels naturally correspond to nonlinear LED carrier rate equations [11], the pruned Volterra model can be configured to emphasize second-order interactions while limiting the number of high-order terms. This is especially relevant in practice, as nonlinear orders higher than two significantly degrade the conditioning of the regression matrix and increase numerical instability.

Finally, the whole model can be written in the form:

$$\hat{y}(n) = \sum_{m_1=-A_1}^{M_1} h_1(m_1)x(n-m_1) + \sum_{m_1=-A_2}^{M_2} \sum_{m_2=m_1}^{M_2} h_2(m_1, m_2)x(n-m_1)x(n-m_2) + \sum_{p=3}^P \sum_{m_1=-A_p}^{M_p} \sum_{m_2=-A_p}^{M_p} h_p(m_1, m_2)x(n-m_1)x(n-m_2)^{p-1} \quad (7)$$

with a number of coefficients equal to

$$N_{\text{coeffs}} = A_1 + M_1 + 1 + \binom{A_2 + M_2 + 2}{2} + \sum_{p=3}^P (A_p + M_p + 1)^2 \quad (8)$$

Since each order has specific domain bounds, the number of hyperparameters of the model increases with the nonlinearity order:

$$N_{\text{hyperparameters}} = 2P + 1$$

III. MODEL TRAINING

Two different optimization problems arise in model training: coefficient estimation and structure optimization. The first searches the best values for the coefficients (also called weights) so that the model best fits the training data. The second one aims at finding the best values for the hyperparameters of the model, defining its structure.

A. Coefficient estimation

The model is intended to act as a predistorter (i.e., at the emitter) but is trained as a postdistorter (i.e., at the receiver), following the indirect learning approach introduced by [18], which is more commonly chosen for DPD model training given its lighter computational cost [4], [10]. In other terms, model training takes place downstream of the distortion and is duplicated upstream of the distortion for practical deployment. This method, which consists in swapping two nonlinear systems and expecting similar results, is not straightforward. Theoretical justification is presented in [19] for any order of a Volterra-derived model, which includes MP and GMP models. This approach is illustrated in Fig. 1.

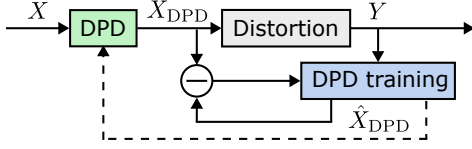


Fig. 1. Indirect learning for digital predistortion.

In order to apply a DPoD or DPD algorithm to mitigate system distortion, we must first train a model to behave as the inverse of the distortion pattern (i.e. to estimate the input vector X from the distorted output vector Y). To do so, we estimate the coefficients of the model, which are contained in the weight vector W , by solving a linear optimization problem:

- 1) Acquire training data (input vector X and output vector Y) from simulation or measurements.
- 2) Train the model by finding W that minimizes the objective function J (the mean square error between estimation and observation):

$$J(W) = \|X - \hat{X}(W)\|_2^2$$

with \hat{X} the estimated input:

$$\hat{X}(W) = \Phi(Y)W$$

with $\Phi(Y)$ the design matrix built from the output vector Y and following the model structure.

The weight vector W can be computed either using the closed-form solution of ordinary least squares (OLS):

$$W = (\Phi^T \Phi)^{-1} \Phi^T Y$$

or with iterative optimization algorithms such as the gradient descent or Newton's method.

- 3) Perform validation on a separate dataset (input X' and output Y') using the estimated weight vector W :

$$J'(W) = \|X' - \hat{X}'(W)\|_2^2$$

with:

$$\hat{X}'(W) = \Phi'(Y')W$$

Proper conditioning of the matrices Φ and $\Phi^T \Phi$ is an important consideration as it heavily impacts the quality and robustness of model training. It mainly depends on the shape of the training data (widely spread and weakly correlated data leads to better training) and the structure of the model: polynomial models often yield coefficients with large disparities in magnitude, which degrades matrix conditioning. Finally, some data preprocessing might be necessary to ensure a relatively low noise level so that the model is trained properly.

B. Structure optimization

The GMP model and the pruned Volterra model structures are defined by several hyperparameters ($P_a, M_a, P_b...$ for the GMP model and $M_1, A_1, M_2...$ for the pruned Volterra model) which must be determined in a different way from the coefficients. Indeed, while coefficients are real-valued unknown parameters within a linear optimization problem, hyperparameters are positive integers defining the number of

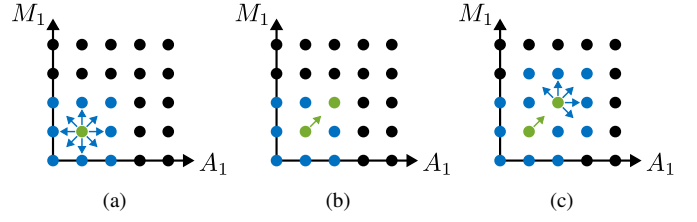


Fig. 2. Illustration of the hill-climbing algorithm (only two dimensions represented here). (a): search in the neighborhood of the starting point. (b): set the optimal point as the new starting point. (c): repeat these two steps until a stop condition is met.

dimensions of the model. The structure of a model with few parameters (e.g., two for MP) can be determined by a straightforward grid search (e.g. by testing each combination with the parameters varying between specified values). However, this method quickly proves too computationally expensive as it scales exponentially with the number of parameters. Consequently, the model structure is usually determined using an iterative search algorithm designed to minimize a criterion that considers both model accuracy and computational complexity.

To achieve this, several methods have been explored, specifically for GMP structure optimization, including artificial bee colony (ABC) optimization, developed in [20], as well as other swarm optimization schemes, as in [21]. The most straightforward method, however, is the hill-climbing (HC) algorithm [9], [22].

While these methods have been specifically designed for the GMP structure optimization, they can be easily adapted to optimize the structure of our pruned Volterra model. The regular version of the HC algorithm is illustrated in Fig. 2 and described as follows:

- 1) Select a starting point of model structure (for example $A_1 = M_1 = A_2 = M_2 = \dots = 1$).
- 2) For each model structure of the neighborhood (-1, 0 or +1 for each parameter), estimate the coefficients of the model and compute the chosen criterion from the validation normalized mean square error (NMSE) and the number of model coefficients ($J = \lambda \times (\text{NMSE} + 20) + N_{\text{coeffs}}$ in [9]) (Fig. 2 (a)).
- 3) Choose the model structure with the lowest criterion value and use it as the new starting point (Fig. 2 (b)).
- 4) Repeat steps 2) and 3) with the neighborhood of the newly chosen point until no neighbor yields a lower criterion value (Fig. 2 (c)).

There exist several alternative versions, as described in [22], including the following:

- Uni-dimensional search: only one parameter changes at a time between the current point and each neighbor.
- First-choice search: once a better neighbor is found, it is directly considered as the new current point without testing the remaining neighbors.

The number of hyperparameters of our pruned Volterra model depends on the order of the model, so we must first choose an order before running the HC algorithm.

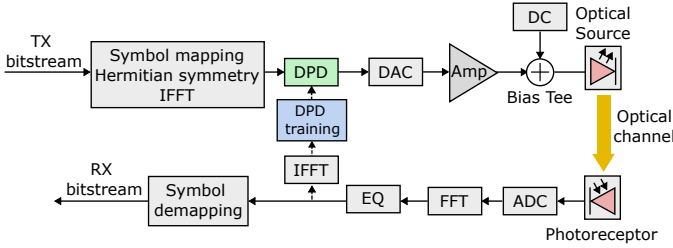


Fig. 3. System chain for digital predistortion.

IV. RESULTS

In this study, the different models are trained offline using measurements from blue 40 μm gallium nitride (GaN) micro-LEDs reported on a 200 mm Silicon substrate. These new GaN-on-silicium micro-LEDs and part of the experimental setup are described in a previous work [23]. Direct current-biased optical orthogonal frequency division multiplexing (DCO-OFDM) with quadrature phase-shift keying (QPSK) modulation is applied to the 512 subcarriers occupying the frequency range from DC to 2.5 GHz. The digital signal is sent to an arbitrary waveform generator (Tektronix AWG5204) with a peak-to-peak voltage set at $V_{pp} = 0.16$ V, then amplified by a low-noise PA (Mini-circuit ZHL1000VH) by 20 dB and DC-biased by a coupler (Picosecond 5575A) at $V_{DC} = 7.8$ V, corresponding to a current density of $J = 2.375$ A/cm². The output light of the micro-LED is then collected using a 200- μm -core, 2-m-long optical fiber (Thorlabs M136L02), that is connected to a high-speed avalanche photoreceiver (Thorlabs APD210). Digital signal acquisition is performed by a high-speed oscilloscope (Tektronix MSO64B). It is worth noting that the nature of OFDM signals is advantageous when performing model training, since it does not introduce significant data correlation and thus improves matrix conditioning. Although the total number of subcarriers for the transmission is 512, we restrict it, depending on the SNR per subcarrier values. This is because subcarriers with a low SNR introduce noise, which disrupts model training. The received signal is equalized by zero-forcing using the mean of successive channel estimations on all OFDM symbols. Equalization (EQ) normalizes the signal and removes linear and time-independent effects, enabling the models to focus on nonlinear behaviors instead of compensating for the linear effects. While this first channel estimation scheme is hardly realistic (using all symbols), it highlights the additional gain brought by DPoD once only the nonlinear effects are remaining. A more realistic channel estimation scheme is discussed at the end of this section. The system chain is illustrated in Fig. 3.

Once EQ is performed, the model can be trained as a postdistorter to be then used as a predistorter, as described in Section III-A. However, the current results are obtained from DPoD only (e.g. from the validation of the *DPD training* block in Fig. 3). DPD validation on the optical bench will be conducted in upcoming studies. It is worth noting that DPD often yields better results than DPoD, even with DPoD-based training [11], because it mitigates nonlinearities earlier in the system chain and avoids propagation of the distortion.

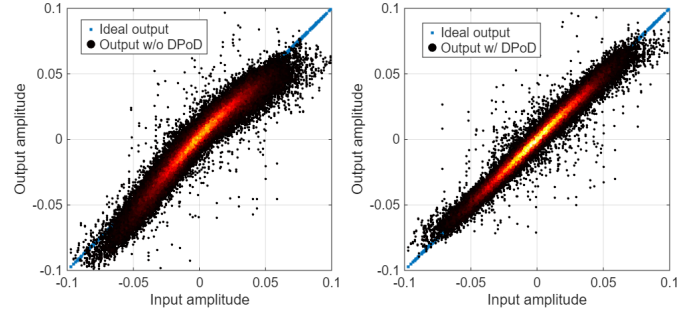


Fig. 4. Channel amplitude-amplitude graphs. Left: received signal with equalization only. Right: received signal with equalization and Volterra-based postdistortion.

The dataset is composed of 206,400 samples from 200 OFDM symbols, with half of the samples used to train the model and half for validation. Running a 30-step unidimensional HC algorithm on the GMP model results in a model with 215 coefficients and the following structure:

$$\begin{aligned} P_a &= 3 & M_a &= 9 \\ P_b &= 3 & M_b &= 4 & L_b &= 9 \\ P_c &= 4 & M_c &= 4 & L_c &= 5 \end{aligned}$$

Running the same algorithm on the third-order pruned Volterra model results in a model with 213 coefficients and the following structure:

$$\begin{aligned} P &= 3 \\ M_1 &= 10 & M_2 &= 13 & M_3 &= 4 \\ A_1 &= 2 & A_2 &= 2 & L_3 &= 3 \end{aligned}$$

From the QPSK transmission, the SNR per subcarrier is estimated with EQ alone and with EQ followed by DPoD. A bit loading algorithm, described in [24], then computes, for each subcarrier, the highest quadrature amplitude modulation (QAM) order resulting in a bit error ratio (BER) below 3.8×10^{-3} , which corresponds to the 7% forward error correction (FEC) limit that ensures proper transmission [12]. We obtain a throughput of 4.30 Gb/s with equalization alone, that is increased to 7.10 Gb/s when applying pruned Volterra-based DPoD, resulting in a throughput gain of 65%. The achieved spectral efficiency over the 1.7 GHz bandwidth is 4.15 b/s/Hz.

The impact of linearization can be observed by the straightening and narrowing of the distortion curve on the amplitude-amplitude (AM-AM) graphs (cf. Fig. 4) and the narrowing of the clusters on the constellation graphs (cf. Fig. 5). The BER versus throughput graph is displayed in Fig. 7. The improvement of the SNR and throughput with distortion mitigation can be observed in Fig. 6. The NMSE, error vector magnitude (EVM), channel capacity and throughput for the MP, GMP, and Volterra models are summarized in Table II.

Fig. 8 shows that the presented model appears more robust to noisy data compared to the MP and GMP models, particularly when high subcarriers with a low SNR (< 0 dB) are introduced. These subcarriers add noise into the observation data, which degrades the training of the MP and GMP models. The enhanced robustness of the proposed approach is primarily attributed to the improved conditioning of the pruned

TABLE II
MODEL PERFORMANCE METRICS.

| | No DPoD | MP | Improvement | GMP | Improvement | Presented Model | Improvement |
|------------|-----------|-----------|-------------|-----------|-------------|-----------------|-------------|
| NMSE | -10.98 dB | -12.66 dB | -1.68 dB | -14.52 dB | -3.54 dB | -15.08 dB | -4.10 dB |
| EVM | -5.53 dB | -6.58 dB | -1.05 dB | -7.56 dB | -2.02 dB | -7.77 dB | -2.23 dB |
| Capacity | 7.02 Gb/s | 8.11 Gb/s | 15.67 % | 9.50 Gb/s | 35.37 % | 9.78 Gb/s | 39.42 % |
| Throughput | 4.30 Gb/s | 5.38 Gb/s | 24.97 % | 6.81 Gb/s | 58.23 % | 7.10 Gb/s | 65.04 % |

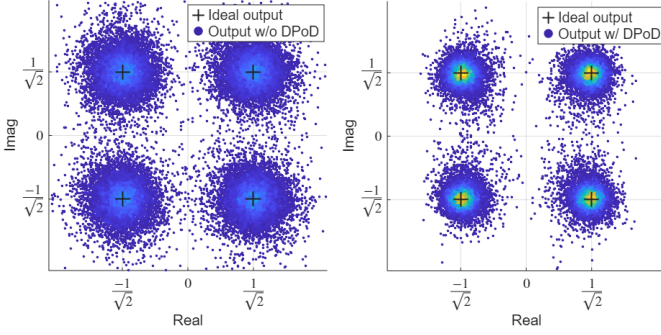


Fig. 5. Constellation graphs. Left: received signal with equalization only. Right: received signal with equalization and Volterra-based postdistortion.

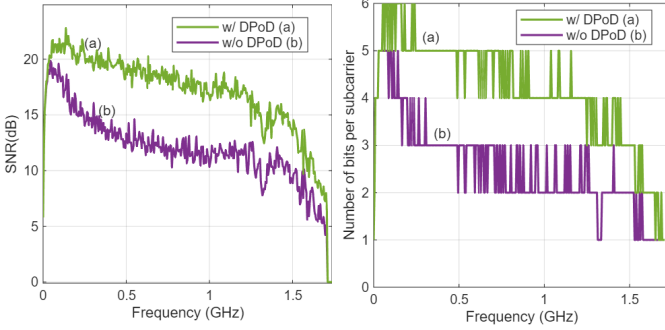


Fig. 6. Left: signal-to-noise ratio by subcarrier graph. Right: number of allocated bits per carrier.

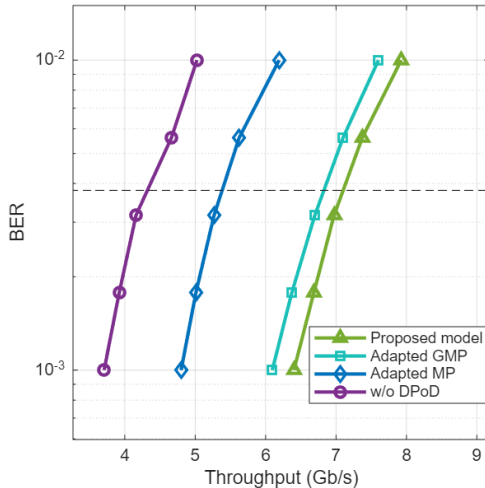


Fig. 7. Bit error rate vs throughput with 350 subcarriers.

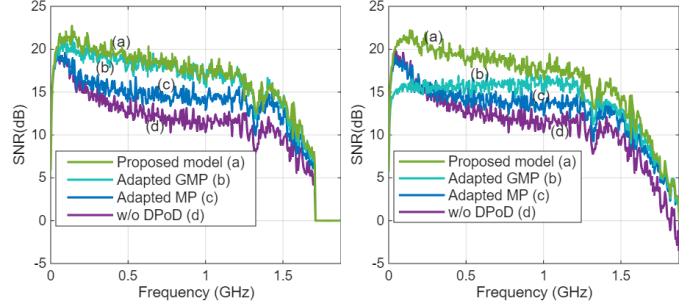


Fig. 8. Comparison of signal-to-noise ratio per subcarriers with different models used as postdistorters. Left: 350 subcarriers. Right 384: subcarriers.

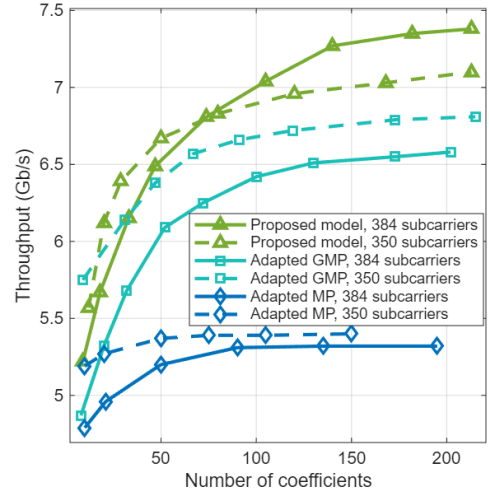


Fig. 9. Throughput vs number of model coefficients.

Volterra's design matrix, which reduces noise amplification during parameter estimation. The condition number of the pruned Volterra's design is on the order of 10^7 , whereas that of the GMP's design matrix is on the order of 10^{19} , which confirms the claims made in Section II-C about model conditioning. The proposed model therefore allows for a higher throughput, e.g., by increasing the number of considered subcarriers (384 instead of 350). In this case, the throughput increases from 4.32 Gb/s with EQ alone to 7.38 Gb/s with EQ and DPoD, resulting in a throughput gain of 71%. Similarly, the energy per bit is reduced from 69 pJ/bit to 40 pJ/bit, representing a comparable relative improvement. To the best of our knowledge, this is the best gain brought by a distortion compensation scheme on a micro-LED optical transmission. Although the obtained energy consumption remains higher

than the best results reported in the literature (see Table I), the observed relative improvement suggests that significantly lower values could be achieved by applying these distortion compensation schemes to more efficient optical components. Furthermore, the linearization extends the usable range of the DC bias voltage, enabling a broader selection of bias values for the joint optimization of energy efficiency and throughput. Future work will focus on a more detailed optimization of energy efficiency.

Additionally, we can consider a more realistic channel estimation using only an 8-OFDM symbol preamble, which corresponds to an overhead of only 4% with respect to the 200-symbol payload. In this case, the throughput increases from 3.95 Gb/s without DPoD to 6.00 Gb/s with our novel pruned Volterra-based model. This performance exceeds that reported in [11], resulting in a throughput and energy efficiency improvement of 52%.

The impact of the number of parameters on the performance of the models is displayed in Fig. 9. It clearly shows that the novel proposed model outperforms the adapted GMP and MP models for any number of coefficients. Moreover, for more than 75 coefficients, the novel proposed model benefits from additional low-SNR subcarriers whereas on the contrary GMP and MP performance is degraded. Finally, we implemented the model from [11] to compare it with the proposed pruned Volterra model using a comparable number of coefficients. Using the model from [11], a throughput and energy efficiency improvement of 24% (from 4.32 Gb/s to 5.36 Gb/s) was achieved with 46 coefficients. This result is consistent with the performance reported in [11], as summarized in Table I. By contrast, with a similar number of 47 coefficients, the proposed pruned Volterra model achieved a throughput and energy efficiency improvement of 57% (from 4.32 Gb/s to 6.78 Gb/s).

V. CONCLUSION

This work presents the first adaptation of the GMP model to direct current-biased optical orthogonal frequency division multiplexing (DCO-OFDM) driven high-speed micro-LED-based OC and introduces a novel pruned Volterra model, yielding enhanced throughput and robustness compared to the GMP model. The results include a 71% increase in throughput on a real time transmission, from 4.32 Gb/s to 7.38 Gb/s, highlighting how these digital processing schemes could improve high-speed and energy-efficient micro-LED-based transmissions. These results show a significant improvement compared to previous work on mitigation of micro-LED distortion, and position this work within the broader effort to design more sustainable systems with greater emphasis on energy efficiency.

Future work will include model validation in a DPD context, transmissions with QAM modulation with varying orders to validate the bit loading algorithm, a study of model complexity for a real-time hardware implementation as well as further studies on model robustness. Applications of the models on micro organic light-emitting diode (OLED) devices will also be conducted to increase data rate and energy efficiency of micro-OLED-based transmissions.

ACKNOWLEDGMENT

This work is part of the HISOPE project that has received funding from the HORIZON-EIC-2023-PATHFINDER-CHALLENGES-01-04 call under grant agreement No 101161573 and from UK Research and Innovation (UKRI) under the UK government's Horizon Europe funding Guarantee (grant numbers 1020583 and 10126101).

REFERENCES

- [1] A. Alexeev, J.-P. M. G. Linnartz, K. Arulandu, and X. Deng, "Characterization of dynamic distortion in LED light output for optical wireless communications," *Photonics Research*, vol. 9, no. 6, p. 916, Jun. 2021. [Online]. Available: <https://opg.optica.org/abstract.cfm?URI=prj-9-6-916>
- [2] L. Ding, G. Zhou, D. Morgan, Z. Ma, J. Kenney, J. Kim, and C. Giardina, "A Robust Digital Baseband Predistorter Constructed Using Memory Polynomials," *IEEE Transactions on Communications*, vol. 52, no. 1, pp. 159–165, Jan. 2004. [Online]. Available: <http://ieeexplore.ieee.org/document/1264205/>
- [3] Z. Dunn, M. Yearly, C. Fulton, and N. Goodman, "Memory polynomial model for digital predistortion of broadband solid-state radar amplifiers," in *2015 IEEE Radar Conference (RadarCon)*. Arlington, VA, USA: IEEE, May 2015, pp. 1482–1486. [Online]. Available: <http://ieeexplore.ieee.org/document/7131230/>
- [4] D. Morgan, Z. Ma, J. Kim, M. Zierdt, and J. Pastalan, "A Generalized Memory Polynomial Model for Digital Predistortion of RF Power Amplifiers," *IEEE Transactions on Signal Processing*, vol. 54, no. 10, pp. 3852–3860, Oct. 2006. [Online]. Available: <http://ieeexplore.ieee.org/document/1703853/>
- [5] W. Chen, X. Liu, J. Chu, H. Wu, Z. Feng, and F. M. Ghannouchi, "A Low Complexity Moving Average Nested GMP Model for Digital Predistortion of Broadband Power Amplifiers," *IEEE Transactions on Circuits and Systems I: Regular Papers*, vol. 69, no. 5, pp. 2070–2083, May 2022. [Online]. Available: <https://ieeexplore.ieee.org/document/9715719/>
- [6] A. Zhu and T. Brazil, "An adaptive Volterra predistorter for the linearization of RF high power amplifiers," in *2002 IEEE MTT-S International Microwave Symposium Digest (Cat. No.02CH37278)*. Seattle, WA, USA: IEEE, 2002, pp. 461–464 vol.1. [Online]. Available: <https://ieeexplore.ieee.org/document/1011655/>
- [7] C. S. Hemsí and C. M. Panazio, "Sparse Flexible Reduced-Volterra Model for Power Amplifier Digital Pre-Distortion," *IEEE Access*, vol. 10, pp. 121 970–121 984, 2022. [Online]. Available: <https://ieeexplore.ieee.org/document/9955534/>
- [8] M. Laakso, A. A. Dowhuszko, and R. Wichman, "Predistortion of OFDM signals for VLC systems using phosphor-converted LEDs," in *2022 IEEE 23rd International Workshop on Signal Processing Advances in Wireless Communication (SPAWC)*. Oulu, Finland: IEEE, Jul. 2022, pp. 1–5. [Online]. Available: <https://ieeexplore.ieee.org/document/9833916/>
- [9] J. E. Sime, P. Morel, M. Telescu, N. Tanguy, and S. Azou, "Digital Predistortion for CO-OFDM Systems Using Generalized Memory Polynomials," in *2020 IEEE Eighth International Conference on Communications and Electronics (ICCE)*. Phu Quoc Island, Vietnam: IEEE, Jan. 2021, pp. 7–11. [Online]. Available: <https://ieeexplore.ieee.org/document/9352081/>
- [10] Y. Bao, Z. Li, J. Li, X. Feng, B.-o. Guan, and G. Li, "Nonlinearity mitigation for high-speed optical OFDM transmitters using digital predistortion," *Optics Express*, vol. 21, no. 6, p. 7354, Mar. 2013. [Online]. Available: <https://opg.optica.org/oe/abstract.cfm?uri=oe-21-6-7354>
- [11] D. Sun, J. Bojarczuk, Z. Jin, M. Marzecki, X. Cui, P. Tian, and G. Stepniak, "6 Gbps Micro-LED Transmission Using OFDM With Predistortion and Single-Tap Nonlinearity Compensation," *IEEE Photonics Technology Letters*, vol. 35, no. 14, pp. 781–784, Jul. 2023. [Online]. Available: <https://ieeexplore.ieee.org/document/10130636/>
- [12] M. S. Islim, R. X. Ferreira, X. He, E. Xie, S. Videv, S. Viola, S. Watson, N. Bamiedakis, R. V. Penty, I. H. White, A. E. Kelly, E. Gu, H. Haas, and M. D. Dawson, "Towards 10 Gb/s orthogonal frequency division multiplexing-based visible light communication using a GaN violet micro-LED," *Photonics Research*, vol. 5, no. 2, p. A35, Apr. 2017. [Online]. Available: <https://opg.optica.org/abstract.cfm?URI=prj-5-2-A35>

- [13] Z. Wei, Z. Liu, X. Liu, L. Wang, L. Wang, C. Yu, and H. Y. Fu, "8.75 gbps visible light communication link using an artificial neural network equalizer and a single-pixel blue micro-led," *Opt. Lett.*, vol. 46, no. 18, pp. 4670–4673, Sep. 2021. [Online]. Available: <https://opg.optica.org/ol/abstract.cfm?URI=ol-46-18-4670>
- [14] D. M. Maclure, C. Chen, J. J. D. McKendry, E. Xie, J. Hill, J. Herrnsdorf, E. Gu, H. Haas, and M. D. Dawson, "Hundred-meter Gb/s deep ultraviolet wireless communications using AlGaIn micro-LEDs," *Optics Express*, vol. 30, no. 26, p. 46811, Dec. 2022. [Online]. Available: <https://opg.optica.org/abstract.cfm?URI=oe-30-26-46811>
- [15] Z. Rao, X. Shan, G. Wang, Z. Jin, R. Lin, X. Cui, R. Liu, K. Xu, and P. Tian, "10.5 Gbps Visible Light Communication Systems Based on C-Plane Freestanding GaN Micro-LED," *Journal of Lightwave Technology*, vol. 42, no. 13, pp. 4360–4364, Jul. 2024. [Online]. Available: <https://ieeexplore.ieee.org/document/10428001/>
- [16] Z. Xie, B. Liu, W. Liu, Q. Chen, and D. Zhu, "A Novel Approach to Pruning Volterra Models with Memory Effects," in *2011 International Conference of Information Technology, Computer Engineering and Management Sciences*. Nanjing, Jiangsu, China: IEEE, Sep. 2011, pp. 59–61. [Online]. Available: <http://ieeexplore.ieee.org/document/6113584/>
- [17] R. N. Braithwaite, "Pruning strategies for a Volterra series model used in digital predistortion (DPD) of RF power amplifiers," in *2017 IEEE Topical Conference on RF/Microwave Power Amplifiers for Radio and Wireless Applications (PAWR)*. Phoenix, AZ, USA: IEEE, Jan. 2017, pp. 4–7. [Online]. Available: <http://ieeexplore.ieee.org/document/7875558/>
- [18] C. Eun and E. Powers, "A new Volterra predistorter based on the indirect learning architecture," *IEEE Transactions on Signal Processing*, vol. 45, no. 1, pp. 223–227, Jan. 1997. [Online]. Available: <https://ieeexplore.ieee.org/document/552219>
- [19] R. de Figueiredo, "The volterra and wiener theories of nonlinear systems," *Proceedings of the IEEE*, vol. 70, no. 3, pp. 316–317, 1982.
- [20] P. Deepak, C. V. Lohith, D. Ramgopal, R. Sanjika Devi, and D. G. Kurup, "Identification of Optimal Generalized Memory Polynomial Structure of RF Power Amplifiers Using Artificial Bee Colony optimization," in *2020 International Conference on Communication and Signal Processing (ICCSP)*. Chennai, India: IEEE, Jul. 2020, pp. 1331–1334. [Online]. Available: <https://ieeexplore.ieee.org/document/9182317/>
- [21] A. Abdelhafiz, L. Behjat, and F. M. Ghannouchi, "Generalized Memory Polynomial Model Dimension Selection Using Particle Swarm Optimization," *IEEE Microwave and Wireless Components Letters*, vol. 28, no. 2, pp. 96–98, Feb. 2018, publisher: Institute of Electrical and Electronics Engineers (IEEE). [Online]. Available: <http://ieeexplore.ieee.org/document/8245868/>
- [22] S. Wang, M. A. Hussein, O. Venard, and G. Baudoin, "A Novel Algorithm for Determining the Structure of Digital Predistortion Models," *IEEE Transactions on Vehicular Technology*, vol. 67, no. 8, pp. 7326–7340, Aug. 2018. [Online]. Available: <https://ieeexplore.ieee.org/document/8354701/>
- [23] S. El Badaoui, L. Maret, N. Delaunay, A. Cibié, P. Le Maitre, C. Ballot, J. Simon, B. Miralles, B. Aventurier, P. De Martino, S. Jacob, and Y. Le Guennec, "Data Communication Using Blue GaN-on-Si Micro-LEDs Reported on a 200-mm Silicon Substrate," *IEEE Photonics Technology Letters*, vol. 36, no. 18, pp. 1149–1152, Sep. 2024. [Online]. Available: <https://ieeexplore.ieee.org/document/10654359/>
- [24] T. Quazi and H. Xu, "Performance analysis of adaptive M-QAM over a flat-fading Nakagami-m channel," *South African Journal of Science*, vol. 107, no. 1/2, Jan. 2011. [Online]. Available: <https://sajs.co.za/article/view/10076>